Computational exploration of Sarin and simulants adsorption on a series of transition metal embedded graphene

Julien Claudot, Estelle Soubeyrand-Lenoir, Guillaume Maurin

Computational exploration of Sarin and simulants adsorption on a series of transition metal embedded graphene

Julien Claudot [a], Estelle Soubeyrand-Lenoir[b], Guillaume Maurin[a*]

[a] ICGM, Univ. Montpellier, CNRS, ENSCM, Montpellier, France

[b] DGA Maîtrise NRBC, BP N°3-5 rue Lavoisier, 91710 Vert le Petit, France.

Abstract

The adsorption of Sarin was systematically explored on a series of transition metal (Zinc, Copper, Molybdenum, Vanadium and Chromium) embedded graphene by Density Functional Theory calculations. These computations revealed that carbon systems impregnated with Chromium, and to a lesser extent, with Molybdenum and Vanadium show very high affinity towards this chemical warfare agent. *In-depth* analysis of the interactions in this embedded carbon/sarin system delivered an unprecedented understanding of the mechanism that governs the capture of sarin by this class of materials further envisioning next generation impregnated carbon-based adsorbents for military and civilian protective devices. As a further stage, three other molecules, Dimethyl methylphosphonate, Hydrogen Cyanide and Cyclohexane were further explored with the objective to identify the most reliable simulant to accurately capture the strength of interactions between real toxic molecules and carbon-based adsorbents.

Keywords: Graphene; Embedded transition Metal; Chemical Warfare Agents; Adsorption; Density functional theory

* Corresponding author mail: guillaume.maurin1@umontpellier.fr

1. Introduction

Chemical warfare agents (CWAs) represent a serious threat to human health if inhaled or if skin happens to be in contact with. They are classified in categories according to the physiological manner they affect the human body, i.e. blister agents or vesicants, chocking agents, riot control agents among others [1]. Specifically, Nerve agents, substances that disrupt the chemical communications through the nervous system, are categorized as persistent and non-persistent substances that relate to their volatility leading to G-series, V-series and T- series [2]. Sarin, the most typical G-nerve agent, is a high volatile Organophosphorus molecule and induces non-persistent to semi-persistent effects, causing death. The potential for terrorist use of this chemical agent has been a concern since its production during the World War I [3]. This was confirmed with the Tokyo gas attacks in 1995 [4] and nowadays, fears are also expressed regarding its use in the Syrian region. Though, terrorist use of sarin on civilian target is viewed as a low probability event, its consequences might be dramatic. Therefore, protection and detection of chemical agents is still a major concern for authorities. Several strategies have been explored to detect and capture sarin [5, 6]. Adsorption of this CWA by porous materials has been envisaged as one of the most efficient approaches. Indeed, many families of adsorbents including metal-organic frameworks (MOFs) [7-10], zeolites [11], hexagonal boron nitrides[12-17] and more intensively activated carbons [18-22] have been explored in this research area. Carbon-based materials present many advantages in the field of adsorption such as large surface area to ensure high adsorption uptake, good chemical stability to allow a long-term use, tunability of their chemical features by grafting diverse functional groups to target the adsorption of polar molecules, and a relatively reasonable cost for further processing. They exhibit however low affinity for certain molecules and they suffer from poor selectivity. In order to address these limitations, one can take advantage of the defects present on the carbon-based structures, such as monovacancy or divacancies [23], by doping this material with transition metal atoms [24-31] with the objective to strengthen the interactions between the adsorbent and a target molecules we wish to capture [32-36]. In the field of respiratory protection devices, activated carbons are currently used for military and civilian purposes to filter the air breath by the user [37, 38]. Most of the experimental and theoretical studies have been dedicated to assess the lifetime of commercial activated carbons for the capture of different types of organic volatile compounds considered as simulants to CWAs [37, 39, 40]. In this context, the theoretical exploration has been limited to the use of macroscopic models implying equations mostly parameterized empirically [38]. In contrast, the microscopic mechanism that drives the capture of contaminants and in particular CWA molecules adsorbed on activated carbons has been only scarcely investigated so far [41, 42].

In the field of CWA capture, the commonly used activated carbons, obtained from the calcination of organic components, such as coconut [43, 44] are impregnated mostly with Chromium to enhance their affinity towards a given toxic molecule [45, 46]. Since Chromium

in most of its forms, can be harmful for human health [47], there is a need to find alternative solution with the possible use of less toxic metals. In this context, here we propose an unprecedented systematic computational investigation to deliver an *in-depth* knowledge at the microscopic scale of the interactions between Chromium embedded carbon and sarin and to further predict the adsorption behaviours of a series of alternative metal atoms to envisage the next generation CWA adsorbents. This computational effort involves Density Functional Theory (DFT) calculations applied to periodic systems made of a single graphene layer embedding one metal atom. This carbon-based model has been selected as a model representative system to provide first insight into the interactions between this CWA and the carbon adsorbents that are currently integrated into protection masks for military purposes. This choice of models is in line with most of the previous studies dealing with the interactions between diverse molecules and carbons [23, 48-51]. Moreover, since the adsorption of sarin on activated carbons is extremely challenging to characterize experimentally due to its hazardousness, a few potential simulants of this CWA were considered in order to identify the most suitable ones to mimic the strength of interactions between the real molecule and the carbon substrates. Typically, we explored dimethyl methylphosphonate (DMMP) [50, 52, 53] which is usually employed as a simulant to explore catalytic oxidation processes [48, 49, 54, 55] and on the other hand, cyclohexane (C_6H_{12}) [56] and hydrogen cyanide (HCN) [51, 57-59], two volatile organic compounds [18, 60] that have been previously considered as simulants to predict the lifetime of respiratory protection devices.

2. Computational details

The DFT calculations were performed using the Quantum Espresso package [61] with the Generalized Gradient Approximation GGA/PBE [62] for the exchange-correlation functional and the DFT+D2 [63] dispersion corrections for the treatment of the van der Waals (vdWs) interactions involved in graphene type systems [64]. Ultrasoft pseudopotentials developped by Vanderbilt [65] were considered to describe the ion cores of atoms. An energy cut-off of 80 Ry was applied in combination with a convergence criteria on the energy of 1×10^{-5} Ry. A Gaussian smearing with $\sigma = 0.01$ was employed for the transition metals, i.e. Zinc (Zn), Copper (Cu), Molybdenum (Mo), Vanadium (V) and Chromium (Cr). A defective graphene model was constructed by removing one carbon atom at the center of the model, this mono-vacancy being then occupied by each transition metal atom mentioned above. Two different simulation boxes were considered depending on the dimensions of the guest molecules. 5×5 graphene sheet ($12.30\text{Å} \times 12.30\text{Å}$) and 4×4 graphene sheet ($9.84\text{Å} \times 9.84\text{Å}$) models embeding a single metal atom, labelled Metal@graphene, were considered for Sarin/Dimethyl methylphosphonate(DMMP) and Hydrogen cyanide (HCN)/Cyclohexane (C_6H_{12}) respectively. A length of 20Å along the z-direction was considered to avoid interactions between their periodically replicated images while Monkhorst-Pack grids of k-

points were used. Different starting configurations for the guest molecules were probed to ensure the convergence towards the lowest energetic arrangements. For comparison the molecule/pure graphene systems were equally considered.

The adsorption energy (E_{ad}) for each molecule was further derived using the following equation :

$$E_{ad} = E_{Molecule-Metal@graphene} - (E_{Molecule} + E_{Metal@graphene})$$

where $E_{Molecule-Metal@graphene}$ is the energy of the DFT-optimized Metal@graphene/molecule complex while $E_{molecule}$ and $E_{Metal@graphene}$ correspond to the single point energy of the single adducts.

Moreover, geometry optimizations of the sarin/Cr@graphene complex, were performed using two other approaches to assess the impact of the applied DFT-methodology (i) Gaussian orbitals cluster based calculations using the PBE [66] exchange-correlation functional with D2 dispersion correction and a TZVP [67] basis set for all atoms as implemented in the Gaussian 09 program suite [68]. (ii) Gaussian Plane Wave (GPW) periodic based calculations as implemented in CP2K [69] code using also the PBE-D2 functional/dispersion correction. **Fig. S1 and S2** reports the resulting optimized sarin/Cr@graphene geometries and adsorption energies using both approaches that concur very well with the results obtained using the periodic DFT plane-wave optimized structures and energetics discussed above.

Further analysis was performed including the calculations of the electronic charge transfer between the metal and the molecules using the Bader formalism [70] as well as the projected density of states (PDOS) for all metal@graphene systems. Bader charges have been computed using 11 valence electrons for Cu, 12 valence electrons for Zn, 13 valence electrons for V and 14 valence electrons for both Mo and Cr.

3. Results and Discussion

Fig. 1 reports the DFT optimized structures for all Metal@graphene models. One can observe that all metal atoms form three bonds with the neighboring carbon atoms while they translate out-of-the-plane consistent with what has been previously reported for diverse metals including first-row transition metals such as Ti and Cu [36, 71-75].

We further evidenced that there is a significant charge transfer from the metal atom to the graphene layer as shown by the corresponding Bader Analysis reported in **Table 1**. This electron density transfer mostly takes place between the metal and its three bonded-carbon atoms. The more positively charged metal atoms are thus expected to establish stronger interactions with the guest molecules than the neutral metal atom. **Table 1** suggests that the

embedded Mo, V and Cr metal which carries the highest positively charge, +1.12e, +1.29e and +1.12e respectively will give rise to the higher affinity towards guest molecules compared to Zn and Cu which exhibit lower charges, i.e. +0.87e and +0.67e respectively.

Fig.2 shows the most stable configurations for sarin in each Metal@graphene model. This CWA molecule adopts a conformation in such a way to preferentially interact with the metal atom via the oxygen atom of its P=O group associated with characteristic oxygen-metal distances ranging from 2.00 to 2.19 Å. Sarin shows however a slightly different adsorption behavior in the case of Cu@graphene with an orientation towards the graphene sheet that allows a side interaction between its fluorine atom and Cu (**Fig.2 (c)**). Moreover, one can note that upon adsorption Zn and Cu are shifted out-of-the plane while the positions of Mo, V and Cr remain almost unchanged. This is clearly indicated by **Table S1** which reports the angle formed between two carbon atoms of the graphene sheet and the metal. These observations have been confirmed by considering different initial orientations for sarin. For comparison, **Fig.2 (a)** reports the case of pure graphene where both its oxygen and fluorine atoms point towards the carbon sheet with characteristic separating distance of 3.03 Å and 3.10 Å respectively.

The corresponding sarin/carbon substrate adsorption energy is reported in **Fig.3** as a function of the nature of the embedded metal. It appears that the stronger interactions are observed in the cases of Mo, V and Cr (-38.95; -43.00 and -43.84 kcal.mol^{-1} respectively), the increase of the adsorption energy within this series of metal being correlated to a shortening of the Metal-oxygen distance (**Fig. 2 (d-f)**). The Cu version leads to a significantly lower adsorption energy (-26.65 kcal.mol^{-1}), implying that the side interaction between the metal and the fluorine atom of sarin (**Fig.2 (c)**) tends to weaken the energetics of the CWA/carbon sheet system. This also holds true for Zn@graphene (-28.32 kcal.mol^{-1}) although the distance between the metal and the oxygen atom of sarin is similar to that observed for Mo, V and Cr. This first series of calculations clearly evidences that Cr, Mo and V metals once embedded in graphene induce a drastic enhancement of the affinity of the carbon-based material for sarin by at least a factor 5 compared to the pure graphene as expected from the higher positively charge behavior reported for these metals. This trend is consistent with the current use of metal impregnated carbons as selective adsorbents to selectively trap CWAs [76, 77].

As a further step, we explored the adsorption of DMMP in each Metal@graphene system. **Fig.4** represents the corresponding most stable configurations. One can observe that similarly to sarin, DMMP preferentially interacts via the oxygen atom of its P=O group pointing towards the metal while in most cases there are side interactions between the metal and the methyl group of DMMP. The metal-dependence of the resulting DMMP adsorption energy is reported in **Fig.3.** Here again, the increase of the adsorption energy observed for Mo, V and Cr (-32.68, -37.67 and -38.94 kcal.mol^{-1} respectively) correlates well with a shortening of the Metal-oxygen distance (2.18 Å, to 2.05 Å and 1.99 Å respectively) while the Zn and Cu versions exhibit lower adsorption energies. Interestingly, DMMP shows not only the same energetics sequence than sarin but also agrees reasonably well the

magnitude of the interactions for all Metal@graphene systems within a 10% range. This observation clearly supports that DMMP is an appropriate simulant to sarin in order to mimic its strength of interactions with carbon-based adsorbents.

To gain further insight into the molecule/metal@graphene complexes, we carefully analyzed their total Density of States (DOS) and Projected Density of States (PDOS) on different orbitals of the atoms of the substrate and Sarin. Typically, Cr@graphene and Zn@graphene have been considered to represent the two distinct categories of embedded metal@graphene models which differ from their CWA energetics point of view. **Fig. 5 (a)** reports the PDOS for the sarin adsorbed on Cr@graphene which is compared to that calculated for the single sarin and Cr@graphene adducts. DOS is projected in such a way to represent the contribution of the orbitals of each interacting atom, i.e. p-orbitals of O atoms for sarin, s - and p-orbitals of C atoms for graphene and s- p- and d-orbitals of the metal atom.

For Cr@graphene, d- states of Cr atoms are mostly localized around the Fermi level with the presence of a peak associated to hybridization with p- orbitals of C atoms of the graphene sheet. This hybridization is made possible due to the out-of-plane position occupied by the metal atom with respect to the graphene sheet discussed above. The d- states of Mo and V, for which the atomic positions are similar to that of Cr, present the same hybridization at the Fermi level with p- orbitals of carbons (see **Fig. S4** and **S5**). On the other hand, one can note a significant shift of the d- states of Zn for Zn@graphene at lower energy level (**Fig. 5 (b))**, this situation being also observed for Cu@graphene (see **Fig. S3**). This absence of hybridization between these two metals and carbon atoms of graphene leads to a larger out-of-plane position of the metal embedded in presence of an adsorbed molecule as presented in **Fig. 2**.

Fig.5a further evidences that once Cr@graphene interacts with sarin, there is a broadening of the d-states of the metal. In particular, the peak situated initially at around 1 eV shifts to higher energies and this can be identified as a signature of the overlap between the d- states of Cr with the high energy p- states of the O atom of sarin around 2.5 eV. In the case of Zn@graphene (**Fig. 5b**), the broadening of d- states of Zn appears at lower energy, around -7 eV, where low energy p- states of the O atom of sarin contribute. This shift between d-states of Cr and Zn complexes at lower energies emphasizes the weaker interactions for sarin/Zn@graphene, providing support to the adsorption energy sequence presented in **Fig. 2**. One can observe that the PDOS above the Fermi energy is mostly composed by p- orbitals of O and C atoms respectively. Though, it is not shown in this figure, p- orbitals of P and s-orbitals of H atoms also contribute to this peak at high energy but in a lesser extent.

A Bader charge analysis was further performed for the sarin/metal@graphene complexes and compared to the case of the isolated sarin. The results are summarized in **Table 1**. The only significant change takes place on the metal with a variation of approximately 15 to 20% of their initial charges in the presence of sarin. Regarding sarin/metal@graphene, the

electron density provided by the metals, i.e, 0.19e, 0.14e, 0.24e, 0.19e and 0.17e for Zn, Cu, Mo, V and Cr respectively is delocalized on the set of carbon atoms of the graphene sheet surrounding the metal. A second contribution of the electron density variation arises from the oxygen atom of sarin interacting with the metal. This whole observation supports that the interaction between sarin and the metal@graphene implies only tiny electron density variation in line with a physisorption phenomenon. The same conclusion holds true for DMMP as evidenced in **Table S2.**

Charge density differences for all sarin/metal@graphene systems are further shown in **Fig. 6**. Charge accumulation is mainly observed in the interacting region between the oxygen atom of sarin and the transition metal atom while depletion of the electron density appears mostly along the P-O bond on the sarin as well as along the region formed by the transition metal atom and its three bonded carbons. The intensity of the charge difference in this bonding region for a given isovalue of $\pm 1.5 \times 10^{-3} e.\text{Å}^{-3}$ increases according to the following sequence: Cr@graphene $\sim$ V@graphene, $\sim$ Mo@graphene > Cu@graphene $\sim$ Zn@graphene. This trend fits well with the calculated adsorption energy profile reported in **Fig. 3**.

Fig. 7 reports the charge density difference plots for DMMP adsorbed on both Zn@graphene and Cr@graphene. A similar profile than **Fig. 6** is obtained when DMMP is involved where the intensity is stronger with Cr, especially in the interacting region and the same depletion region can be found along the P-O bond of sarin and below the metal atoms. These similarities confirm that DMMP mimics well sarin in terms of nature and strength of interactions with the metal embedded graphene sheet.

As a further stage, we investigated the adsorption of two other molecules proposed in the past as potential simulants to CWAs [78], i.e. hydrogen cyanide and cyclohexane. In order to thoroughly explore the energy landscape of these systems, three different initial configurations were considered for HCN, i.e. perpendicular to the carbon sheet with either N or H atoms pointing towards the metal or parallel to the carbon sheet, while keeping in all cases the molecule linear. Regarding C_6H_{12}, two configurations were tested with the ring either parallel or perpendicular to the carbon sheet. The cyclic hydrocarbon was evidenced to be preferentially orientated parallel to the carbon sheet for all considered metal@graphene (see **Fig. 8**), the metal interacting with the hydrogen atoms of the ring with characteristic separating distances ranging from 2.17 to 2.22 Å as illustrated for Cr@graphene in **Fig. 8(a)**. Interestingly the corresponding adsorption energy profile reported in **Fig.3** is similar to the trends obtained for sarin and DMMP although the values are far lower, typically for Cr@graphene the adsorption energies for C_6H_{12} and DMMP are -8.01 and -38.94 kcal.mol^{-1} respectively. This makes the choice of cyclohexane as CWA simulant questionable at least from an energetics standpoint.

Regarding HCN, we observed that the preferential configuration corresponds mostly to the case of N atom pointing towards the metal as illustrated in **Fig. 8** for Zn, Cu, V and Cr

embedded atoms with characteristic N-Metal distances ranging from 1.95 to 2.13 Å. However, in the case of Mo, a HCN geometry parallel to the carbon sheet was found to be as stable as the perpendicular conformation, the total electronic energy difference between these structures being very small (see **Table S3**). However, to maintain a systematic exploration of the adsorption energies, **Fig. 3** reports the adsorption energies corresponding to the perpendicular orientation of the molecule for all metal@graphene systems. The so-calculated energetics profile is shown to reproduce very well that of sarin associated with a physisorption process. Notably, the simulated adsorption energy values for HCN match very well those for DMMP, thus suggesting that HCN can be equally considered as a reliable simulant for sarin.

Fig. 9 presents the charge density difference plots for all HCN/metal@graphene systems. One can note that the intensity of the charge accumulation on the N atom is different in the case of Zn/Cu (**Fig. 9 (a-b)**) compared to Mo/V/Cr (**Fig. 9 (c-d-e))**. While this latter group of metal shows a predominant charge accumulation in the region of the N atom of HCN, it is not anymore the case for Zn and Cu which both show a high electron density at the vicinity of carbon atoms of the graphene. This electronic density variation is the reason behind the strongest interactions occurring in the Mo, V or Cr@graphene. Regardless of this difference, all metal@graphene attract charges from HCN because of high electron density surrounding its cyano-group.

4. Summary

The interactions between 3d (Zn, Cu, V, Cr) and 4d (Mo) transition metals embedded carbons and sarin as well as three different simulants were explored computationally. DFT calculations confirmed that the use of Cr metal is highly attractive for CWA capture owing to the resulting very high interaction energies with both sarin, DMMP and HCN. Meanwhile, alternative metals like Mo and V show an affinity for these molecules as high as Cr. This paves the way towards to the impregnation of these less toxic metals into next generation carbon-based adsorbents to ensure an efficient capture of CWAs by physisorption. Our computations also strongly suggest that cyclohexane, currently used as simulant to CWA to assess the lifetime of carbon-based adsorbents might be not so relevant since this molecule does not allow to capture the correct magnitude of the interactions that involve sarin with such adsorbents. This is a critical point since such a distinct energetics is expected to make significant changes in terms of not only the capture but also on the desorption process which is of utmost importance for the regeneration of the adsorbents.

Acknowledgements

The research leading to these results has received funding from the DGA Maîtrise NRBC.

References

[1] T.T. Marrs, R.L. Maynard, F. Sidell, Chemical warfare agents: toxicology and treatment, John Wiley & Sons, 2007.
[2] R.T. Delfino, T.S. Ribeiro, J.D. Figueroa-Villar, Organophosphorus compounds as chemical warfare agents: a review, Journal of the Brazilian Chemical Society, 20 (2009) 407-428.
[3] A. Mangerich, C. Esser, Chemical warfare in the First World War: reflections 100 years later, Archives of toxicology, 88 (2014) 1909-1911.
[4] T. Okumura, N. Takasu, S. Ishimatsu, S. Miyanoki, A. Mitsuhashi, K. Kumada, K. Tanaka, S. Hinohara, Report on 640 victims of the Tokyo subway sarin attack, Annals of emergency medicine, 28 (1996) 129-135.
[5] P. Kowalczyk, P.A. Gauden, A.P. Terzyk, A.V. Neimark, Screening of carbonaceous nanoporous materials for capture of nerve agents, Physical Chemistry Chemical Physics, 15 (2013) 291-298.
[6] C. Montoro, F. Linares, E. Quartapelle Procopio, I. Senkovska, S. Kaskel, S. Galli, N. Masciocchi, E. Barea, J.A. Navarro, Capture of nerve agents and mustard gas analogues by hydrophobic robust MOF-5 type metal–organic frameworks, Journal of the American Chemical Society, 133 (2011) 11888-11891.
[7] C. Vieira Soares, G. Maurin, A.A. Leitão, Computational Exploration of the Catalytic Degradation of Sarin and Its Simulants by a Titanium Metal–Organic Framework, The Journal of Physical Chemistry C, 123 (2019) 19077-19086.
[8] C.V. Soares, A. Leitão, G. Maurin, Computational evaluation of the chemical warfare agents capture performances of robust MOFs, Microporous and Mesoporous Materials, 280 (2019) 97-104.
[9] I. Matito-Martos, P.Z. Moghadam, A. Li, V. Colombo, J.A. Navarro, S. Calero, D. Fairen-Jimenez, Discovery of an optimal porous crystalline material for the capture of chemical warfare agents, Chemistry of Materials, 30 (2018) 4571-4579.
[10] M. Agrawal, D.F. Sava Gallis, J.A. Greathouse, D.S. Sholl, How useful are common simulants of chemical warfare agents at predicting adsorption behavior?, The Journal of Physical Chemistry C, 122 (2018) 26061-26069.
[11] E. Güvenç, M.G.k. Ahunbay, Adsorption of methyl tertiary butyl ether and trichloroethylene in MFI-type zeolites, The Journal of Physical Chemistry C, 116 (2012) 21836-21843.
[12] R. Baierle, T. Schmidt, A. Fazzio, Adsorption of CO and NO molecules on carbon doped boron nitride nanotubes, Solid State Communications, 142 (2007) 49-53.
[13] M.D. Ganji, A. Mirnejad, A. Najafi, Theoretical investigation of methane adsorption onto boron nitride and carbon nanotubes, Science and technology of advanced materials, 11 (2010) 045001.
[14] S.-H. Jhi, Y.-K. Kwon, Hydrogen adsorption on boron nitride nanotubes: a path to room-temperature hydrogen storage, Physical Review B, 69 (2004) 245407.

[15] X. Wu, J. Yang, X.C. Zeng, Adsorption of hydrogen molecules on the platinum-doped boron nitride nanotubes, The Journal of chemical physics, 125 (2006) 044704.
[16] X. Wu, X.C. Zeng, Adsorption of transition-metal atoms on boron nitride nanotube: A density-functional study, The Journal of chemical physics, 125 (2006) 044711.
[17] Y. Xie, Y.-P. Huo, J.-M. Zhang, First-principles study of CO and NO adsorption on transition metals doped (8, 0) boron nitride nanotube, Applied Surface Science, 258 (2012) 6391-6397.
[18] A. Junkaew, C. Rungnim, M. Kunaseth, R. Arróyave, V. Promarak, N. Kungwan, S. Namuangruk, Metal cluster-deposited graphene as an adsorptive material for m-xylene, New Journal of Chemistry, 39 (2015) 9650-9658.
[19] K.-J. Kim, C.-S. Kang, Y.-J. You, M.-C. Chung, M.-W. Woo, W.-J. Jeong, N.-C. Park, H.-G. Ahn, Adsorption–desorption characteristics of VOCs over impregnated activated carbons, Catalysis Today, 111 (2006) 223-228.
[20] S. Wang, H. Ang, M.O. Tade, Volatile organic compounds in indoor environment and photocatalytic oxidation: state of the art, Environment international, 33 (2007) 694-705.
[21] J. Dai, J. Yuan, P. Giannozzi, Gas adsorption on graphene doped with B, N, Al, and S: a theoretical study, Applied Physics Letters, 95 (2009) 232105.
[22] D. Kaplan, L. Shmueli, I. Nir, D. Waysbort, I. Columbus, Degradation of adsorbed sarin on activated carbons: a 31P-MAS-NMR study, CLEAN–Soil, Air, Water, 35 (2007) 172-177.
[23] I.A. Pašti, A. Jovanović, A.S. Dobrota, S.V. Mentus, B. Johansson, N.V. Skorodumova, Atomic adsorption on graphene with a single vacancy: systematic DFT study through the periodic table of elements, Physical Chemistry Chemical Physics, 20 (2018) 858-865.
[24] C.-Y. Lu, M.-Y. Wey, Simultaneous removal of VOC and NO by activated carbon impregnated with transition metal catalysts in combustion flue gas, Fuel Processing Technology, 88 (2007) 557-567.
[25] L. Hu, X. Hu, X. Wu, C. Du, Y. Dai, J. Deng, Density functional calculation of transition metal adatom adsorption on graphene, Physica B: Condensed Matter, 405 (2010) 3337-3341.
[26] S. Jungsuttiwong, Y. Wongnongwa, S. Namuangruk, N. Kungwan, V. Promarak, M. Kunaseth, Density functional theory study of elemental mercury adsorption on boron doped graphene surface decorated by transition metals, Applied Surface Science, 362 (2016) 140-145.
[27] E.J. Santos, A. Ayuela, D. Sánchez-Portal, First-principles study of substitutional metal impurities in graphene: structural, electronic and magnetic properties, New Journal of Physics, 12 (2010) 053012.
[28] H. Wang, Q. Wang, Y. Cheng, K. Li, Y. Yao, Q. Zhang, C. Dong, P. Wang, U. Schwingenschlögl, W. Yang, Doping monolayer graphene with single atom substitutions, Nano letters, 12 (2011) 141-144.
[29] S. Gupta, N. Dimakis, Computational predictions of electronic properties of graphene with defects, adsorbed transition metal-oxides and water using density functional theory, Applied Surface Science, 467 (2019) 760-772.
[30] M. Rafique, Y. Shuai, H.-P. Tan, H. Muhammad, Theoretical perspective on structural, electronic and magnetic properties of 3d metal tetraoxide clusters embedded into single and di-vacancy graphene, Applied Surface Science, 408 (2017) 21-33.
[31] A.V. Markevich, M. Baldoni, J.H. Warner, A.I. Kirkland, E. Besley, Dynamic behavior of single Fe atoms embedded in graphene, The Journal of Physical Chemistry C, 120 (2016) 21998-22003.

[32] C. Ramos-Castillo, J. Reveles, R. Zope, R. De Coss, Palladium clusters supported on graphene monovacancies for hydrogen storage, The Journal of Physical Chemistry C, 119 (2015) 8402-8409.
[33] M. Kunaseth, T. Mudchimo, S. Namuangruk, N. Kungwan, V. Promarak, S. Jungsuttiwong, A DFT study of arsine adsorption on palladium doped graphene: effects of palladium cluster size, Applied Surface Science, 367 (2016) 552-558.
[34] Y.-H. Lu, M. Zhou, C. Zhang, Y.-P. Feng, Metal-embedded graphene: a possible catalyst with high activity, The Journal of Physical Chemistry C, 113 (2009) 20156-20160.
[35] L. Ma, J.-M. Zhang, K.-W. Xu, V. Ji, Hydrogen adsorption and storage on palladium-decorated graphene with boron dopants and vacancy defects: a first-principles study, Physica E: Low-dimensional Systems and Nanostructures, 66 (2015) 40-47.
[36] A. Krasheninnikov, P. Lehtinen, A.S. Foster, P. Pyykkö, R.M. Nieminen, Embedding transition-metal atoms in graphene: structure, bonding, and magnetism, Physical review letters, 102 (2009) 126807.
[37] G.O. Wood, Activated carbon adsorption capacities for vapors, Carbon, 30 (1992) 593-599.
[38] G.O. Wood, J. Stampfer, Adsorption rate coefficients for gases and vapors on activated carbons, Carbon, 31 (1993) 195-200.
[39] G.O. Wood, P. Lodewyckx, An extended equation for rate coefficients for adsorption of organic vapors and gases on activated carbons in air-purifying respirator cartridges, AIHA Journal, 64 (2003) 646-650.
[40] G.O. Wood, Estimating service lives of organic vapor cartridges, American Industrial Hygiene Association Journal, 55 (1994) 11-15.
[41] B.N. Papas, I.D. Petsalakis, G. Theodorakopoulos, J.L. Whitten, CI and DFT Studies of the Adsorption of the Nerve Agent Sarin on Surfaces, The Journal of Physical Chemistry C, 118 (2014) 23042-23048.
[42] N.K. Jaiswal, G. Kovačević, Sarin chemisorbent based on cobalt-doped graphene, Applied Surface Science, 480 (2019) 759-764.
[43] I. Tan, A. Ahmad, B. Hameed, Adsorption of basic dye on high-surface-area activated carbon prepared from coconut husk: Equilibrium, kinetic and thermodynamic studies, Journal of hazardous materials, 154 (2008) 337-346.
[44] S. Babel, T.A. Kurniawan, Cr (VI) removal from synthetic wastewater using coconut shell charcoal and commercial activated carbon modified with oxidizing agents and/or chitosan, Chemosphere, 54 (2004) 951-967.
[45] P. Lodewyckx, Adsorption of chemical warfare agents, in: Interface Science and Technology, Elsevier, 2006, pp. 475-528.
[46] G. Prasad, B. Singh, R. Vijayaraghavan, Respiratory protection against chemical and biological warfare agents, Defence Science Journal, 58 (2008) 686.
[47] M. Costa, C.B. Klein, Toxicity and carcinogenicity of chromium compounds in humans, Critical reviews in toxicology, 36 (2006) 155-163.
[48] M.D. Esrafili, P. Nematollahi, H. Abdollahpour, A comparative DFT study on the CO oxidation reaction over Al-and Ge-embedded graphene as efficient metal-free catalysts, Applied Surface Science, 378 (2016) 418-425.
[49] M.D. Esrafili, N. Saeidi, Sn-embedded graphene: An active catalyst for CO oxidation to CO2?, Physica E: Low-dimensional Systems and Nanostructures, 74 (2015) 382-387.

[50] C. Majumder, Adsorption and decomposition of dimethyl methylphosphonate on pristine and mono-vacancy defected graphene: A first principles study, Applied Surface Science, 418 (2017) 318-327.
[51] H.-K. Dong, Y.-P. Wang, L.B. Shi, First principles study of HCN adsorption on graphene doped with 5d transition metal, Surface Review and Letters, 23 (2016) 1550095.
[52] M.D. Ganji, Z. Dalirandeh, A. Khosravi, A. Fereidoon, Aluminum nitride graphene for DMMP nerve agent adsorption and detection, Materials Chemistry and Physics, 145 (2014) 260-267.
[53] J. Henych, A. Mattsson, J. Tolasz, V. Štengl, L. Österlund, Solar light decomposition of warfare agent simulant DMMP on TiO 2/graphene oxide nanocomposites, Catalysis Science & Technology, 9 (2019) 1816-1824.
[54] J.-Y. Tang, J.-S. Shen, L. Chen, J.-W. Jiang, J. Lu, X. Zhao, G.-L. Dai, Investigation of carbon monoxide catalytic oxidation on vanadium-embedded graphene, Monatshefte für Chemie-Chemical Monthly, 149 (2018) 1349-1356.
[55] X. Liu, Y. Sui, T. Duan, C. Meng, Y. Han, CO oxidation catalyzed by Pt-embedded graphene: A first-principles investigation, Physical Chemistry Chemical Physics, 16 (2014) 23584-23593.
[56] L. Ma, X. Chen, Adsorption of naphthenic acids to the nitrogen-coordinated transition-metal embedded graphene: A DFT study, Russian Journal of Physical Chemistry B, 10 (2016) 1027-1031.
[57] C. Tabtimsai, T. Somtua, T. Motongsri, B. Wanno, A DFT study of H 2 CO and HCN adsorptions on 3d, 4d, and 5d transition metal-doped graphene nanosheets, Structural Chemistry, 29 (2018) 147-157.
[58] A.S. Rad, M.R. Zardoost, E. Abedini, First-principles study of terpyrrole as a potential hydrogen cyanide sensor: DFT calculations, Journal of molecular modeling, 21 (2015) 273.
[59] B. Zeng, W. Li, H. Chen, G. Li, First-principles study on the adsorption of hydrogen cyanide on the Metal-doped (8, 0) Boron Nitride Nanotubes, Chemical Physics Letters, (2019).
[60] M. Kunaseth, P. Poldorn, A. Junkeaw, J. Meeprasert, C. Rungnim, S. Namuangruk, N. Kungwan, C. Inntam, S. Jungsuttiwong, A DFT study of volatile organic compounds adsorption on transition metal deposited graphene, Applied Surface Science, 396 (2017) 1712-1718.
[61] P. Giannozzi, S. Baroni, N. Bonini, M. Calandra, R. Car, C. Cavazzoni, D. Ceresoli, G.L. Chiarotti, M. Cococcioni, I. Dabo, QUANTUM ESPRESSO: a modular and open-source software project for quantum simulations of materials, Journal of physics: Condensed matter, 21 (2009) 395502.
[62] J.P. Perdew, Y. Wang, Accurate and simple analytic representation of the electron-gas correlation energy, Physical Review B, 45 (1992) 13244.
[63] S. Grimme, Semiempirical GGA-type density functional constructed with a long-range dispersion correction, Journal of computational chemistry, 27 (2006) 1787-1799.
[64] Jogender, Mandeep, B. Badhani, R. Kakkar, Adsorption of methyl isocyanate on M-4 (M= Fe, Ni, and Cu) cluster-decorated graphene and vacancy graphene: a DFT-D2 study, STRUCTURAL CHEMISTRY, (2020).
[65] D. Vanderbilt, Soft self-consistent pseudopotentials in a generalized eigenvalue formalism, Physical review B, 41 (1990) 7892.
[66] J.P. Perdew, K. Burke, M. Ernzerhof, Generalized gradient approximation made simple, Physical review letters, 77 (1996) 3865.

[67] A. Schäfer, C. Huber, R. Ahlrichs, Fully optimized contracted Gaussian basis sets of triple zeta valence quality for atoms Li to Kr, The Journal of Chemical Physics, 100 (1994) 5829-5835.
[68] M. Frisch, G. Trucks, H.B. Schlegel, G.E. Scuseria, M.A. Robb, J.R. Cheeseman, G. Scalmani, V. Barone, B. Mennucci, G. Petersson, gaussian 09, Revision d. 01, Gaussian, Inc., Wallingford CT, 201 (2009).
[69] T.D. Kühne, M. Iannuzzi, M.D. Ben, V.V. Rybkin, P. Seewald, F. Stein, T. Laino, R.Z. Khaliullin, O. Schütt, F. Schiffmann, D. Golze, J. Wilhelm, S. Chulkov, M.H. Bani-Hashemian, V. Weber, U. Borštnik, M. Taillefumier, A.S. Jakobovits, A. Lazzaro, H. Pabst, T. Müller, R. Schade, M. Guidon, S. Andermatt, N. Holmberg, G.K. Schenter, A. Hehn, A. Bussy, F. Belleflamme, G. Tabacchi, A. Glöß, M. Lass, I. Bethune, C.J. Mundy, C. Plessl, M. Watkins, J. VandeVondele, M. Krack, J. Hutter, CP2K: An electronic structure and molecular dynamics software package - Quickstep: Efficient and accurate electronic structure calculations, The Journal of Chemical Physics, 152 (2020) 194103.
[70] W. Tang, E. Sanville, G. Henkelman, A grid-based Bader analysis algorithm without lattice bias, Journal of Physics: Condensed Matter, 21 (2009) 084204.
[71] M. Zhou, Y.-H. Lu, Y.-Q. Cai, C. Zhang, Y.-P. Feng, Adsorption of gas molecules on transition metal embedded graphene: a search for high-performance graphene-based catalysts and gas sensors, Nanotechnology, 22 (2011) 385502.
[72] E. Song, Y. Zhu, Q. Jiang, Density functional theory calculations of adsorption of hydrogen fluoride on titanium embedded graphene, Thin Solid Films, 546 (2013) 124-127.
[73] L. Wang, Q. Luo, W. Zhang, J. Yang, Transition metal atom embedded graphene for capturing CO: a first-principles study, International journal of hydrogen energy, 39 (2014) 20190-20196.
[74] J. Sirijaraensre, J. Limtrakul, Hydrogenation of CO2 to formic acid over a Cu-embedded graphene: A DFT study, Applied Surface Science, 364 (2016) 241-248.
[75] D. Mombrú, R. Faccio, A.W. Mombrú, First row transition metal atoms embedded in multivacancies in a rippled graphene system, Applied Surface Science, 435 (2018) 102-107.
[76] A. Somy, M.R. Mehrnia, H.D. Amrei, A. Ghanizadeh, M. Safari, Adsorption of carbon dioxide using impregnated activated carbon promoted by Zinc, International journal of greenhouse gas control, 3 (2009) 249-254.
[77] A. Saxena, B. Singh, A. Sharma, V. Dubey, R.P. Semwal, M.V.S. Suryanarayana, V.K. Rao, K. Sekhar, Adsorption of dimethyl methylphosphonate on metal impregnated carbons under static conditions, Journal of hazardous materials, 134 (2006) 104-111.
[78] J. Lavoie, S. Srinivasan, R. Nagarajan, Using cheminformatics to find simulants for chemical warfare agents, Journal of hazardous materials, 194 (2011) 85-91.

Figure captions

Figure 1 DFT-optimized models for (a) Zn@ graphene (b) Cu@graphene (c) Mo@graphene (d) V@graphene and (e) Cr@graphene (top and side views). C, Zn, Cu, Mo, V and Cr atoms are represented in grey, blue, orange, light blue, green and yellow, respectively.

Figure 2 Most stable DFT-optimized configurations of Sarin on (a) pure Graphene, (b) Zn@ graphene (c) Cu@graphene (d) Mo@graphene (e) V@graphene and (f) Cr@graphene. The reported distances are expressed in Å. C, O, F, P, H, Zn, Cu, Mo, V and Cr atoms are respectively in grey, red, cyan, purple, white, blue, orange, light blue, green and yellow, respectively.

Figure 3 Metal-Dependence of the DFT-calculated adsorption energy (in kcal/mol) for sarin, DMMP, HCN and C_6H_{12} in pure graphene and metal@graphene models.

Figure 4 Most stable DFT-optimized configurations of DMMP on (a) pure Graphene, (b) Zn@ graphene (c) Cu@graphene (d) Mo@graphene (e) V@graphene and (f) Cr@graphene. The reported distances are expressed in Å. C, O, F, P, H, Zn, Cu, Mo, V and Cr atoms are represented in grey, red, cyan, purple, white, blue, orange, light blue, green and yellow, respectively.

Figure 5 Comparison of PDOS for the sarin/Cr@graphene (a) and sarin/ Zn@graphene complexes. For each system panel I, panel II and panel III present PDOS of the isolated sarin, isolated metal@graphene and resulting complexes. Total DOS of molecule, O_p states, C_s (sarin) states, C_p (sarin) states, C_s (graphene) states, C_s (graphene) states, s-, p-, and d- states of metal are represented in black, green, dashed blue, dashed red, blue, red, bold blue, bold red, bold black, respectively.

Figure 6 Charge differences for Sarin/metal@graphene presented with isovalue of $\pm 1.5 \times 10^{-3} e.\text{Å}^{-3}$. (a) Zn@graphene (b) Cu@graphene (c) Mo@graphene, (d) V@graphene and (e) Cr@graphene. Blue and red colors represent the charge accumulation and depletion regions respectively.

Figure 7 Charge differences for DMMP/metal@graphene presented with isovalue of $\pm 1.5 \times 10^{-3} e.\text{Å}^{-3}$.(a) Zn@graphene and (b) Cr@graphene. Blue and red colors represent, respectively, the charge accumulation and depletion regions.

Figure 8 Most stable DFT-optimized configurations of HCN on (a) Cr@graphene and of HCN on (b) Zn@graphene (c) Cu@graphene (d) Mo@graphene, (e) V@graphene and (f) Cr@graphene. The reported distances are expressed in Å. C, H, N, Zn, Cu, Mo, V and Cr atoms are represented in grey, white, dark blue, blue, orange, light blue, green and yellow, respectively.

Figure 9 Charge differences for HCN/metal@graphene presented with isovalue of $\pm 1.5 \times 10^{-3} e.\text{Å}^{-3}$. (a) Zn@graphene (b) Cu@graphene (c) Mo@graphene (d) V@graphene and (e) Cr@graphene. Blue and red colors represent, respectively, the charge accumulation and depletion regions.

Table captions

Table 1 Bader charge analysis for the isolated Sarin and Metal embedded graphene as well as for the Sarin/Metal@graphene systems. Plus and minus signs represent charge increment and charge reduction, respectively. $\sum C$ refers to the sum of Bader charges carried by the 49 carbon atoms composing the graphene.

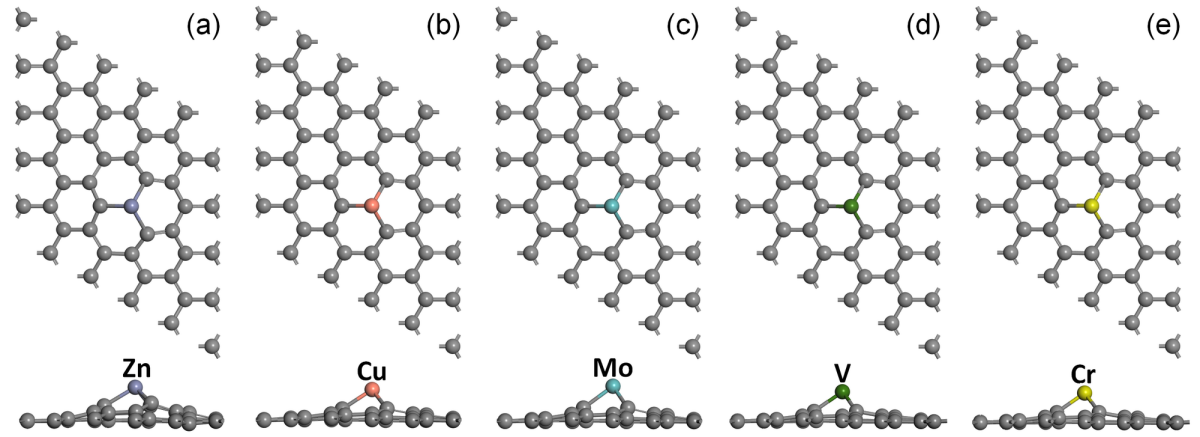
(a)
(b)
(c)
(d)
(e)
Zn
Cu
Mo
V
Cr

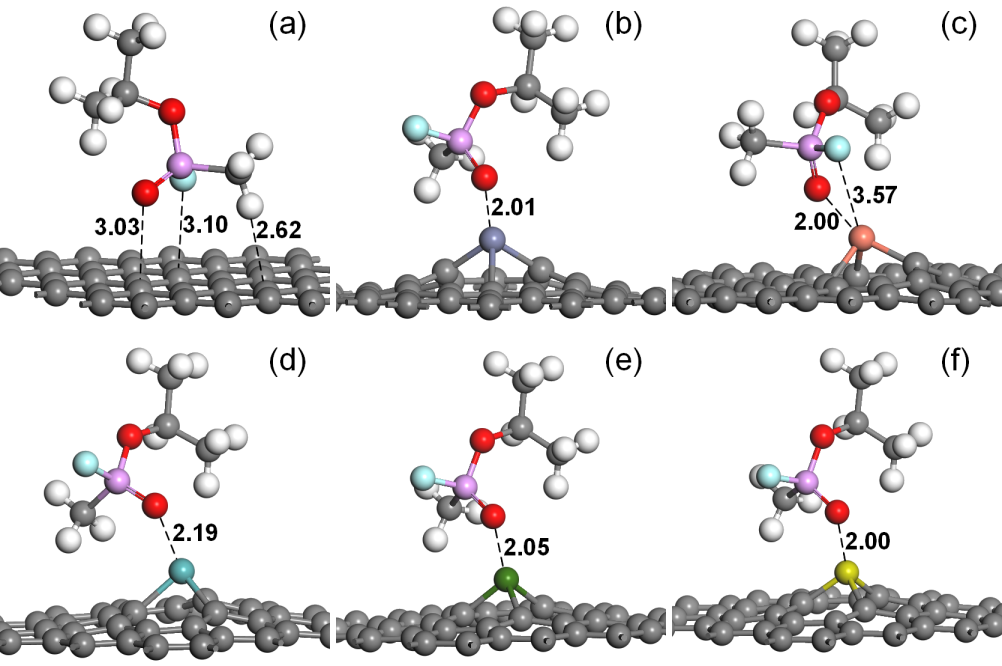
(a)
3.03
3.10
2.62
(b)
2.01
(c)
3.57
2.00
(d)
2.19
(e)
2.05
(f)
2.00

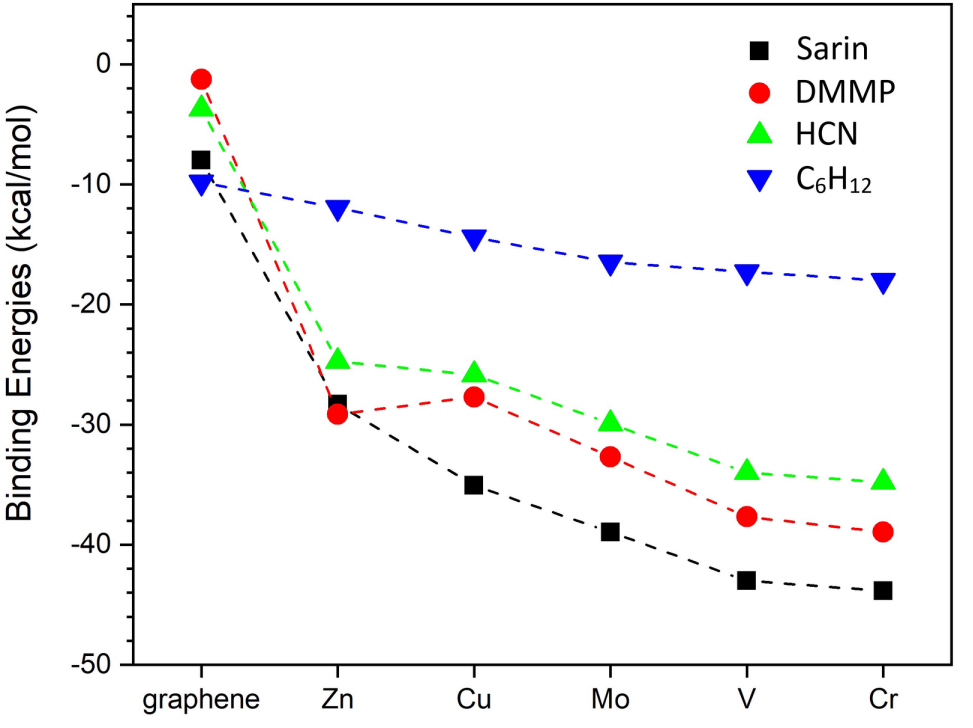
Binding Energies (kcal/mol)
0
-10
-20
-30
-40
-50
graphene
Zn
Cu
Mo
V
Cr
Sarin
DMMP
HCN
C6H12

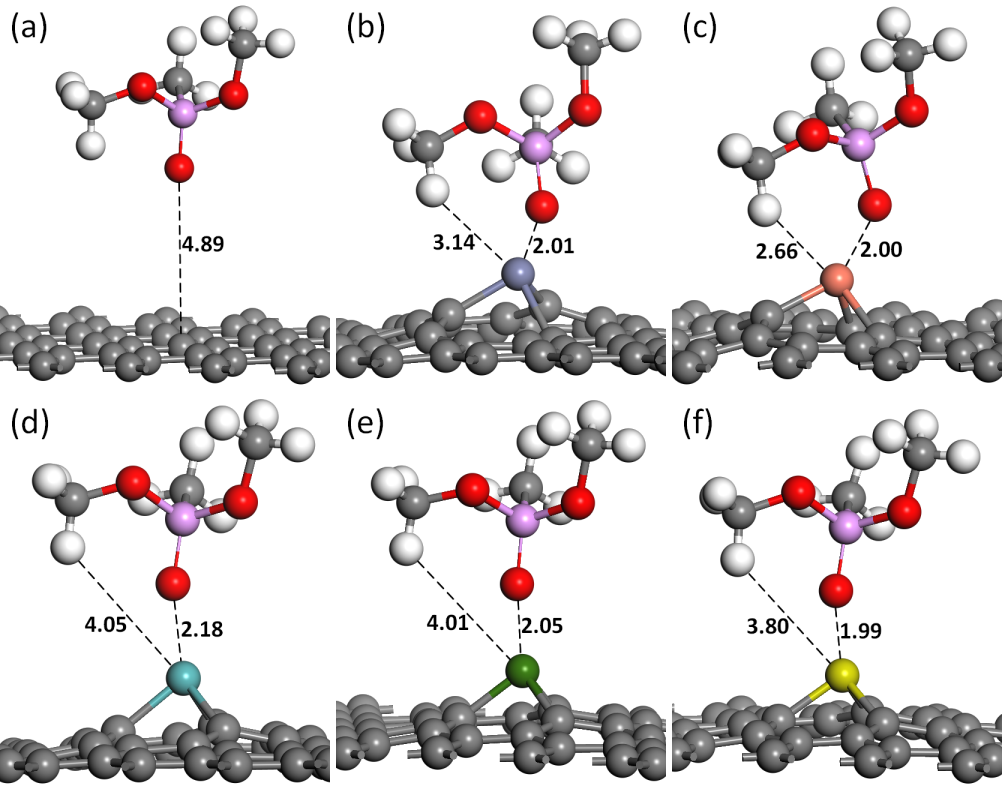
(a)
4.89
(b)
3.14
2.01
(c)
2.66
2.00
(d)
4.05
2.18
(e)
4.01
2.05
(f)
3.80
1.99

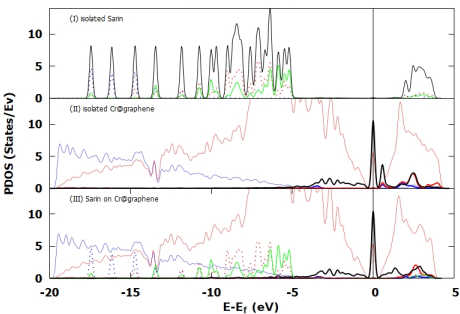
(a) Sarin on Cr@graphene
(I) isolated Sarin
(II) isolated Cr@graphene
(III) Sarin on Cr@graphene
PDOS (States/Ev)
E-Ef (eV)

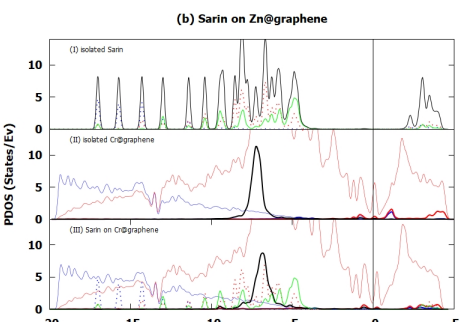
(b) Sarin on Zn@graphene
(I) isolated Sarin
(II) isolated Cr@graphene
(III) Sarin on Cr@graphene
PDOS (States/Ev)
E-Ef (eV)

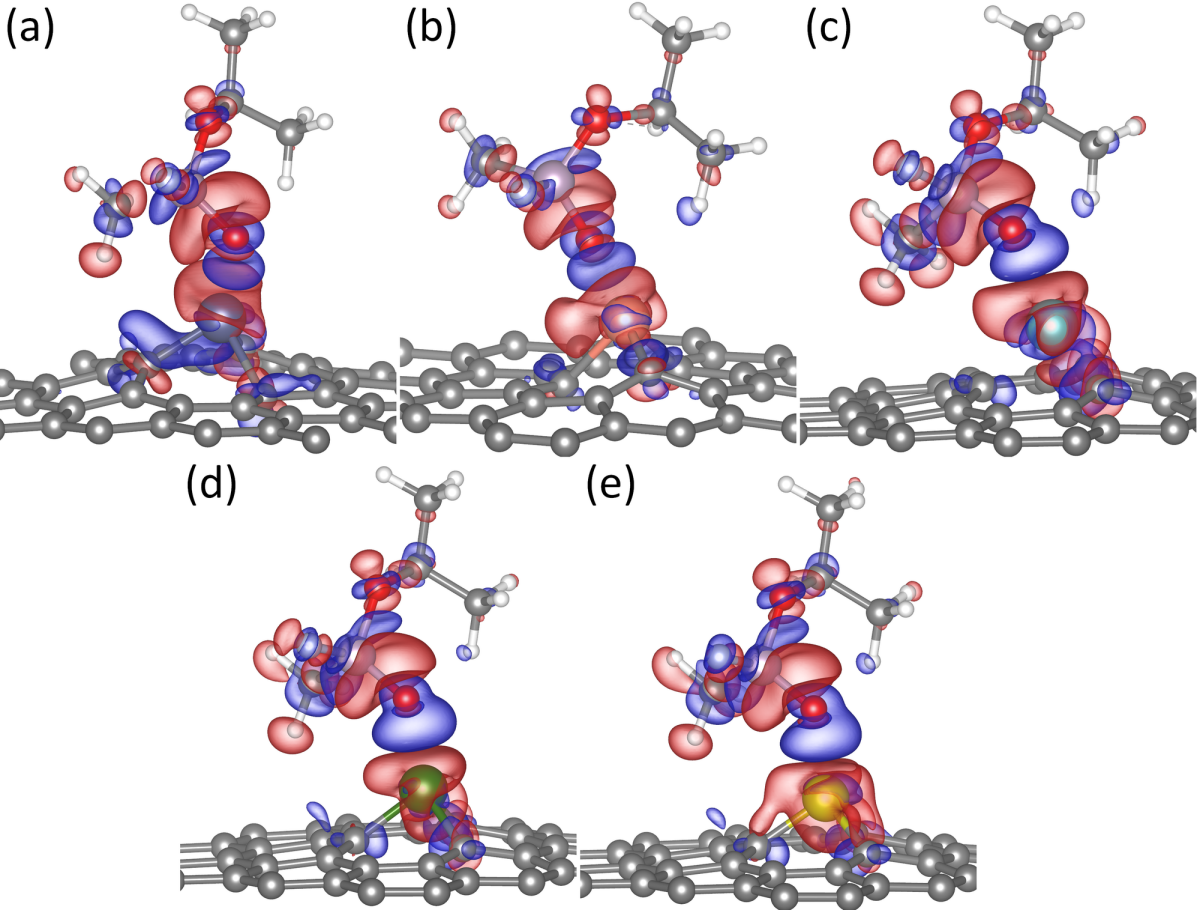
(a)
(b)
(c)
(d)
(e)

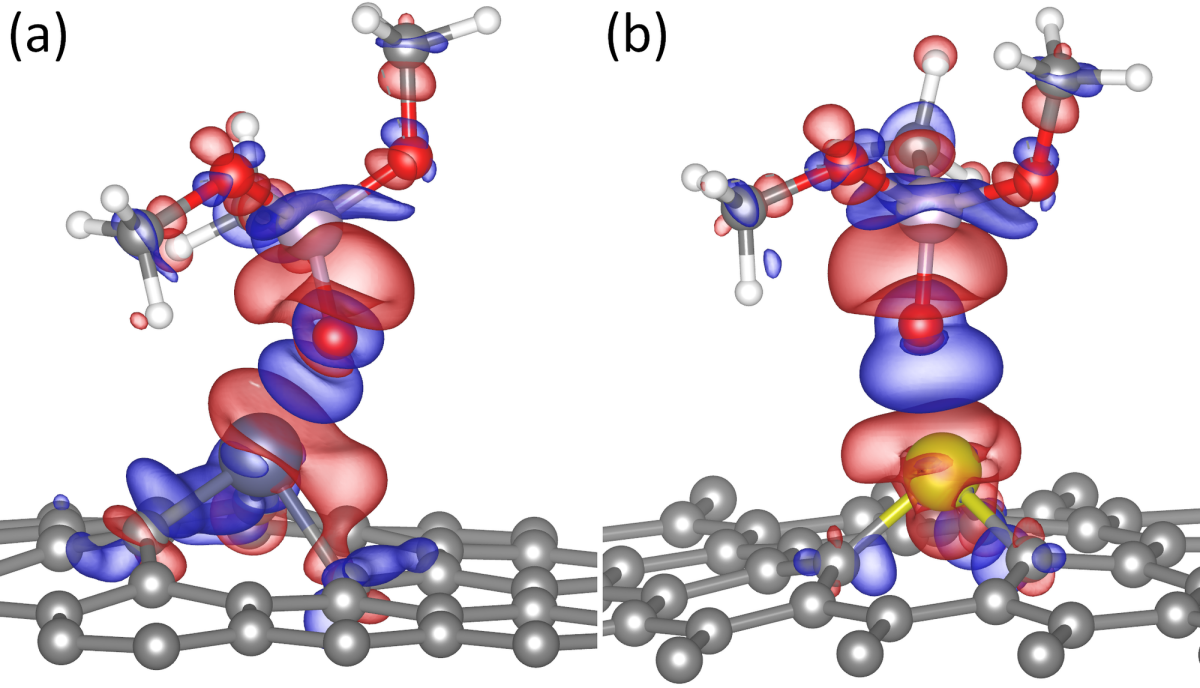
(a)
(b)

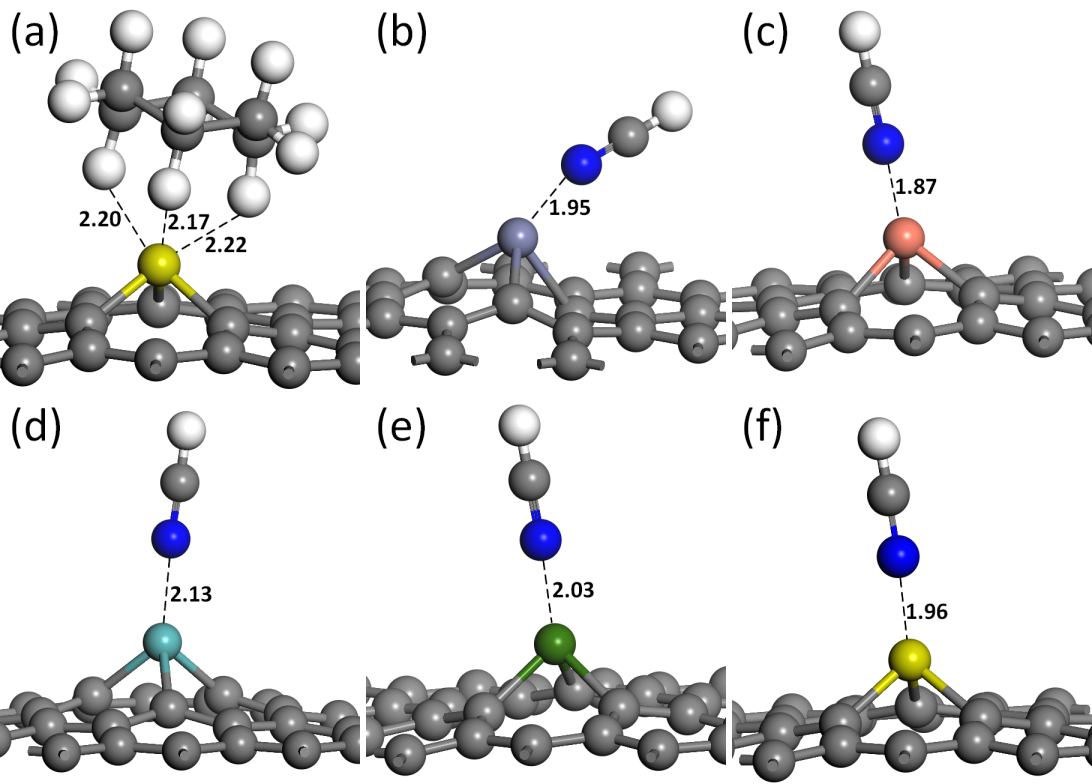
(a)
2.20
2.17
2.22
(b)
1.95
(c)
1.87
(d)
2.13
(e)
2.03
(f)
1.96

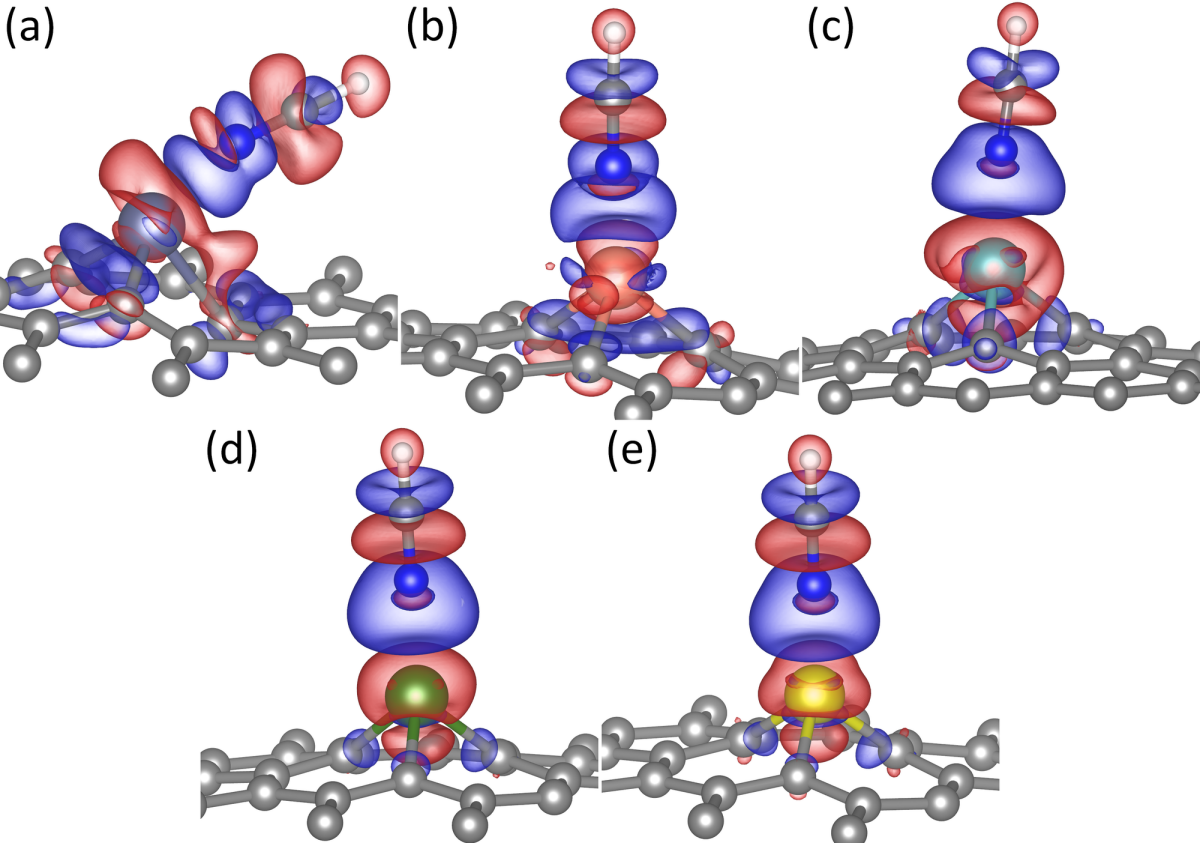
(a)
(b)
(c)
(d)
(e)

		Graphene		Zn@graphene		Cu@graphene	
		Isolated	Adsorbed	Isolated	Adsorbed	Isolated	Adsorbed
Carbon Substrate	Metal	-	-	+0.81	+1.00	+0.63	+0.77
	$\sum C$	-	-	-0.81	-1.08	-0.63	-0.84
Sarin	P	+4.91	+4.91	+4.91	+4.91	+4.91	+4.91
	F	-1.02	-1.03	-1.02	-1.00	-1.02	-1.01
	O =(P)	-1.88	-1.89	-1.88	-1.83	-1.88	-1.84
	O -(CH)	-1.70	-1.71	-1.70	-1.70	-1.70	-1.69
	CH_3 -(P)	-1.00	-1.00	-1.00	-1.00	-1.00	-0.98
		Mo@Graphene		V@graphene		Cr@graphene	
		Isolated	Adsorbed	Isolated	Adsorbed	Isolated	Adsorbed
Carbon Substrate	Metal	+1.10	+1.34	+1.30	+1.49	+1.11	+1.28
	$\sum C$	-1.10	-1.40	-1.30	-1.55	-1.11	-1.36
Sarin	P	+4.91	+4.91	+4.91	+4.91	+4.91	+4.91
	F	-1.02	-1.00	-1.02	-1.00	-1.02	-1.00
	O =(P)	-1.88	-1.84	-1.88	-1.85	-1.88	-1.83
	O -(CH)	-1.70	-1.70	-1.70	-1.69	-1.70	-1.69
	CH_3 -(P)	-1.00	-1.00	-1.00	-0.98	-1.00	-1.00

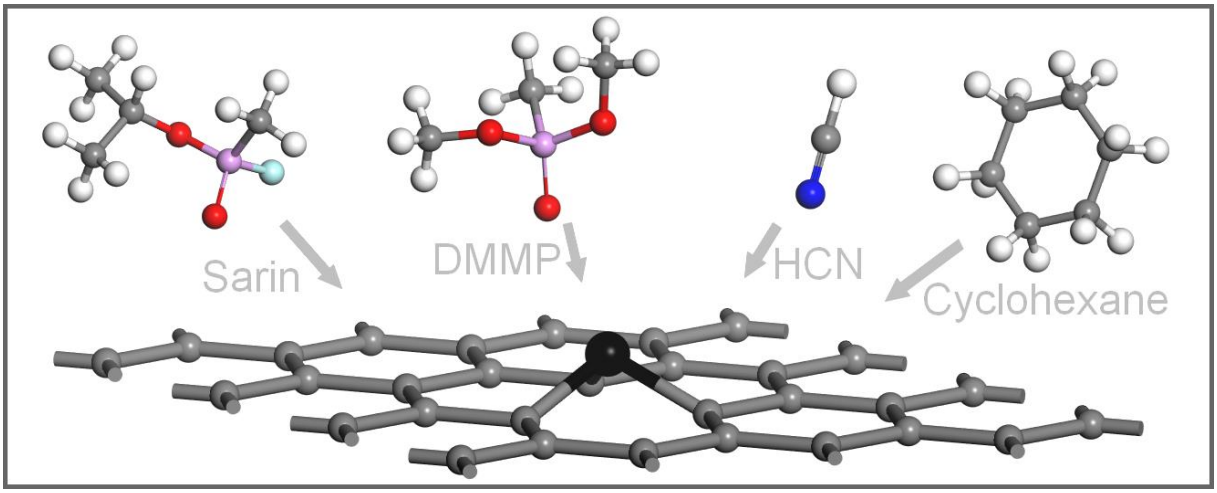
Sarin
DMMP
HCN
Cyclohexane